Shape coexistence in ^{153}Ho

Dibyadyuti Pramanik,[1] S. Sarkar,[1,*] M. Saha Sarkar,[2,†] Abhijit Bisoi,[1] Sudatta Ray,[2,‡] Shinjinee Dasgupta,[2,§] A.Chakraborty,[3] Krishichayan,[4] Ritesh Kshetri,[5] Indrani Ray,[2] S. Ganguly,[6] M. K. Pradhan,[2] M. Ray Basu,[7] R. Raut,[8] G. Ganguly,[7] S.S. Ghugre,[8] A.K. Sinha,[8] S.K. Basu,[9] S. Bhattacharya,[2] A. Mukherjee,[2] P. Banerjee,[2] and A. Goswami[2]

[1] *Indian Institute of Engineering Science and Technology, Shibpur, Howrah - 711103, INDIA*
[2] *Saha Institute of Nuclear Physics, Bidhannagar, Kolkata - 700064, INDIA*
[3] *Visva-Bharati, Santiniketan - 731235, INDIA*
[4] *Duke University, Durham, North Carolina, USA*
[5] *Sidho-Kanho-Birsha University, Purulia - 723101, INDIA*
[6] *Bethune College, Kolkata - 700006, INDIA*
[7] *University of Calcutta, Kolkata - 700073, INDIA*
[8] *UGC-DAE Consortium for Scientific Research, Kolkata- 700098, INDIA*
[9] *Variable Energy Cyclotron Centre, Kolkata - 700064, INDIA*

(Dated: July 26, 2016)

The high-spin states in ^{153}Ho, have been studied by $^{139}_{57}$La(^{20}Ne, 6n) reaction at a projectile energy of 139 MeV at Variable Energy Cyclotron Centre (VECC), Kolkata, India, utilizing an earlier campaign of Indian National Gamma Array (INGA) setup. Data from gamma-gamma coincidence, directional correlation and polarization measurements have been analyzed to assign and confirm the spins and parities of the levels. We have suggested a few additions and revisions of the reported level scheme of ^{153}Ho. The RF-gamma time difference spectra have been useful to confirm the half-life of an isomer in this nucleus. From the comparison of experimental and theoretical results, it is found that there are definite indications of shape coexistence in this nucleus. The experimental and calculated lifetimes of several isomers have been compared to follow the coexistence and evolution of shape with increasing spin.

PACS numbers: 21.10.Re,21.10.Tg, 21.60.Cs,27.30.+t

arXiv:1607.06954v1 [nucl-ex] 23 Jul 2016

I. INTRODUCTION

The neutron deficient rare-earth isotopes near the magic nucleus ^{146}Gd have shown multitude of structural features as functions of neutron number as well as spin [1, 2]. For isotones with N = 86, excitation spectra show single particle nature associated with non-collective modes. For N = 88, strong collectivity in terms of appreciable prolate deformation is manifested in the low-lying spectra. However, even for the nuclei which are very close to ^{146}Gd, although low spin excitations are usually very irregular and complex indicating spherical shape with single or multi-particle excitations, at relatively higher energies superdeformed (SD) bands [1, 3, 4] are observed. The observations indicate that these nuclei are very soft against shape changes. The features have been interpreted theoretically using microscopic shell-model and mean-field descriptions [2]. One of the distinguishing features of this mass region is the existence of an island of high spin isomers [1, 5, 6], which are excited in heavy ion reactions. These isomers can also indicate a sharp change of structural configurations within the same nucleus [5, 6].

This mass region has been investigated extensively particularly for even - even nuclei [1]. It has been possible to observe structural changes and shape coexistence effects for them. Some nuclei in this region, like $^{152}_{66}$Dy$_{86}$ [3, 4], are found to be near-spherical oblate in shape at low spins. However, they exhibit coexisting collective prolate shapes like superdeformation at higher spins. On the other hand there are evidences of excitation pattern in $^{154}_{66}$Dy$_{88}$ similar to collective prolate rotors at low spins which evolve to non collective oblate shape at high spins. Nuclei with higher neutron numbers (N > 90), behave like collective prolate rotors throughout their entire excitation pattern. For odd Z nuclei, like Holmium (Ho), although individual studies of different isotopes [7–11] exist, systematic analysis of the structural evolution of this element with variations in neutron number is scarce. Ho (Z=67) is the nearest odd-Z neighbor of most extensively studied Dy (Z=66). A systematic study [12–18] of the isotopes of Ho element has been initiated to understand how nuclear structure differs due to the addition of a single unpaired proton. In the present work, ^{153}Ho isotope has been studied.

The neutron deficient isotope of Ho, ^{153}Ho has an unpaired proton coupled to the even-even core ^{152}Dy. ^{153}Ho with neutron number N=86 has been studied previously [10, 19, 20] to high spins (J $\simeq$ 81/2) [19]. Its $11/2^-$ ground state quadrupole moment measured using Laser resonance ionization mass spectroscopy (LRIMS) method

*ss@physics.iiests.ac.in
†maitrayee.sahasarkar@saha.ac.in
‡Amity University, Noida - 201303, INDIA
§Heritage Institute of Technology, Anandapur, Kolkata 700107, INDIA

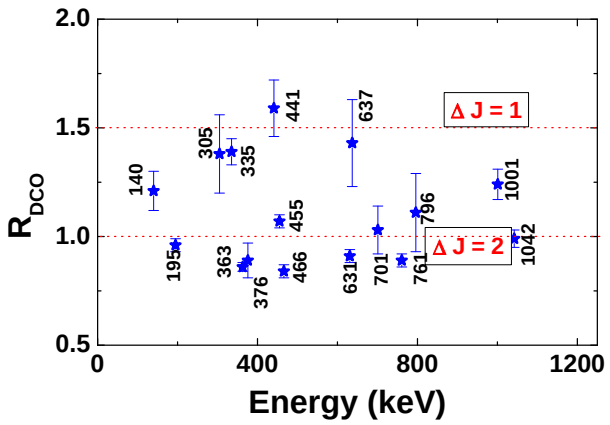

FIG. 1: (Color Online) Experimental DCO ratios (R_{DCO}) for few transitions in ^{153}Ho. Typical values of R_{DCO}s determined for $\Delta J = 0$ and 1 transitions from E2 gated spectra are indicated in the figure by dotted lines.

is negative indicating an oblate shape [21]. Even in the latest compilation [10], there are uncertainties in the spin and parity assignments of the excited levels. In an earlier work [19], the structure of this nucleus has been analyzed phenomenologically in terms of shell model configurations of the excited states. There have been suggestions that the 3^- octupole vibration may play a major role in its structure [19]. In a later study [20], a low deformation collective band in ^{153}Ho has been found to be associated with a triaxial shape with large positive value triaxiality parameter (γ).

In the present work, the high-spin states in ^{153}Ho, populated in a heavy ion reaction have been studied. Data from gamma-gamma coincidence, directional correlation and polarization measurements have been analyzed to assign and confirm the spins and parities of the levels. A few additions and revisions of the reported [19] level scheme of ^{153}Ho have been suggested. The RF-gamma time difference spectra have been used to confirm the half-life of a nanosecond isomer in this nucleus. Total Routhian Surface (TRS) and Particle Rotor Model (PRM) calculations have also been performed. From the comparison of experimental and theoretical results in the entire spin-energy domain, it is demonstrated that there are definite indications of shape coexistence in this nucleus. The comparison of experimental and calculated lifetimes of several isomers observed in the excitation spectra of this nucleus helps in following the shape coexistence and its evolution with increasing spins.

II. EXPERIMENTAL DETAILS AND DATA ANALYSIS

High spin states of ^{153}Ho were populated by bombarding 139 MeV ^{20}Ne beam on a La_2O_3 target at Variable Energy Cyclotron Centre (VECC), Kolkata. The target of thickness $3mg/cm^2$ was prepared by centrifuge method on Al backing of $2.2mg/cm^2$. ^{153}Ho was populated most strongly, along with population of ^{151,152,154}Ho, $^{152-153}$Dy nuclei. Results from preliminary data analysis from this experiment have been reported earlier [12, 14–16]. The experiment has been carried out using one of the earlier campaigns [22] of Indian National Gamma Array (INGA) setup, which comprised of six Compton-suppressed Clover detectors. In this setup, the detectors were placed at $40^o(2)$, $90^o(2)$, $125^o(2)$ with respect to the beam direction. Data were acquired in LIST mode. At least two correlated gamma energies from the Clovers, their time information as well as corresponding RF time information with respect to the master gate have been included in the LIST data.

The energy and efficiency calibration of the Clover detectors have been done using radioactive ^{133}Ba and ^{152}Eu sources. The coincidence events were sorted into two symmetric γ-γ matrices with time gates of 800 ns and 200ns. These matrices are used to generate various background subtracted gated spectra. The matrices were analyzed using the codes INGASORT [23] and RADWARE [24]. To generate background subtracted gated spectra, INGASORT program has been used. In this program, the background is eliminated, on peak by peak basis.

A. Angular Correlation Data Analysis

Angle dependent asymmetric γ-γ matrices have been generated to determine the multipolarity of γ- ray transitions from directional correlation of γ- rays emitted from excited oriented states (DCO) measurements. The DCO ratio (R_{DCO}) of a γ transition (γ_1) is defined as the ratio of intensities of that γ-ray (I_{γ_1}) for two different angles in coincidence with another γ-ray (γ_2) of known multipolarity. It is given by the ratio, defined as

$$R_{DCO} = \frac{I_{\gamma_1} \text{ observed at } 40^\circ, \text{ gated by } \gamma_2 \text{ at } 90^\circ}{I_{\gamma_1} \text{ observed at } 90^\circ, \text{ gated by } \gamma_2 \text{ at } 40^\circ}$$

The DCO ratio of each γ has been obtained by putting a gate on a γ transition of known multipolarity with zero or very small mixing ratio (Fig. 1). For the stretched transitions with same multipolarity as the gating transition, R_{DCO} value should be very close to unity. For different multipolarities of the gating and projected transitions, the R_{DCO} value depends on the angle between the detectors and the amount of mixing present in the mixed multipolarity transition. For the assignment of spins and the γ -ray multipole mixing ratios (δ), the experimental DCO values were compared with the theoretical values calculated by using the computer code ANGCOR [25]. Spin alignment parameter $\sigma/J = 0.3$ was used for this calculation. This choice was guided by several earlier works [26–29]. However, the choice has been also tested further. The experimental mixing ratio of 140 keV gamma determined in the present work has been used to calculate the

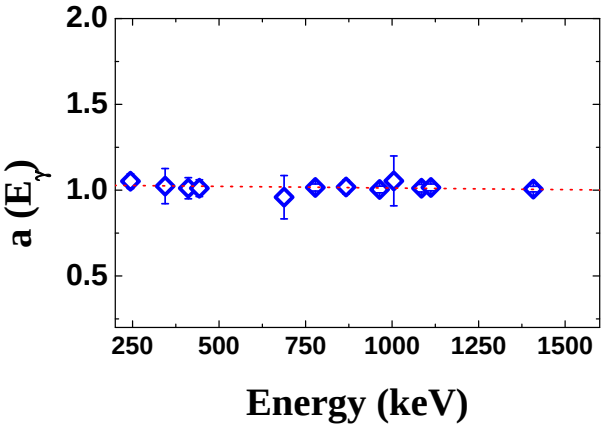

FIG. 2: (Color Online) Asymmetry parameter $a(E_\gamma)$ plotted as a function of energy. The fitted straight line is shown as dotted line in the figure.

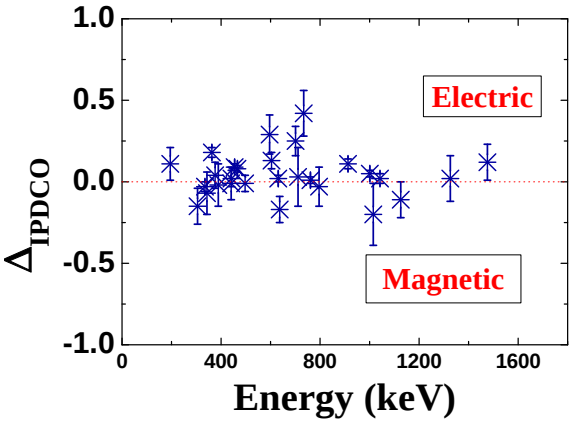

FIG. 3: (Color Online) Polarization symmetry for a few transitions in ^{153}Ho. The dotted line separates the regions corresponding to pure Electric and Magnetic transitions.

K-shell internal conversion coefficient from BrIcc v2.3S Conversion Coefficient Calculator [30] which agrees reasonably well with the experimental K-shell electron conversion coefficient for this transition as reported in Fig. 2 of the reference [19] as well as in [10].

B. Polarization Data Analysis

Integrated polarization asymmetry measurements (IPDCO) have been done to determine the electric or magnetic nature of the γ -ray transitions. Two asymmetric IPDCO matrices were constructed from the data. The first (second) matrix named as parallel (perpendicular) was constructed having on first axis the simultaneous events recorded in the two crystals of the 90^o Clover detector which are parallel (perpendicular) to the emission plane and on the second axis the coincident γ ray registered in any other detector. The polarization asymmetry is defined as

$$\Delta_{IPDCO} = \frac{a(E_\gamma)N_\perp - N_\parallel}{a(E_\gamma)N_\perp + N_\parallel} \quad (1)$$

where $N_\perp$ and $N_\parallel$ are the intensities of the full energy peaks observed in the perpendicular and parallel matrices, respectively. The correction term a(E_γ) is introduced due to asymmetry in the response of the different crystals of the Clover detector at 90^o. It is defined as

$$a(E_\gamma) = \frac{N_\parallel(unpolarized)}{N_\perp(unpolarized)}. \quad (2)$$

In the present experiment a is measured as a function of energy of unpolarized γ-rays from radioactive ^{152}Eu source. Fig.2 shows the variation of a with E_γ and it was fitted with the expression $a(E_\gamma) = a_0 + a_1E_\gamma$ resulting into $a_0 = 1.03$ and $a_1 \sim$ -1.93 $\times 10^{-5}$, where E_γ is in keV.

For determination of experimental polarization asymmetry from each of the IPDCO matrices, we have put gates on γs on the second axis and observed the projected parallel and perpendicular spectra of the 90^o Clover detectors (Fig. 3). A positive (negative) value of Δ_{IPDCO}, indicates a pure electric (magnetic) transition. But for mixed transitions, usually this value is close to zero and the sign varies depending on the extent of mixing.

C. Lifetime data analysis

In this experiment, the RF frequency is $\simeq$5.56 MHz, so the time difference between two consecutive RF pulses from the cyclotron is around 180 ns. Fig. 4 shows the RF-γ time-difference to amplitude converted (TAC) spectrum with γ energies ranging from $\approx$ 100 keV to 4000 keV. This TAC spectrum has been taken within a range of 200 ns. In this condition the resolution of the prompt time spectrum comes out to be $\simeq$ 27.7 ns without any restriction in energy.

III. RESULTS

A. Level Scheme

The level scheme of ^{153}Ho, shown in Fig. 5, has been established using the coincidence relationship, relative intensities, R_{DCO} and Δ_{IPDCO} ratios of γ rays. All transitions above 2772 keV ($31/2^+$) up to $E_x \sim$ 12 MeV and a tentative spin of $81/2^-$ reported in the earlier work by Radford *et al.* [19], have been observed in the present experiment. The transitions below the long - lived iso-

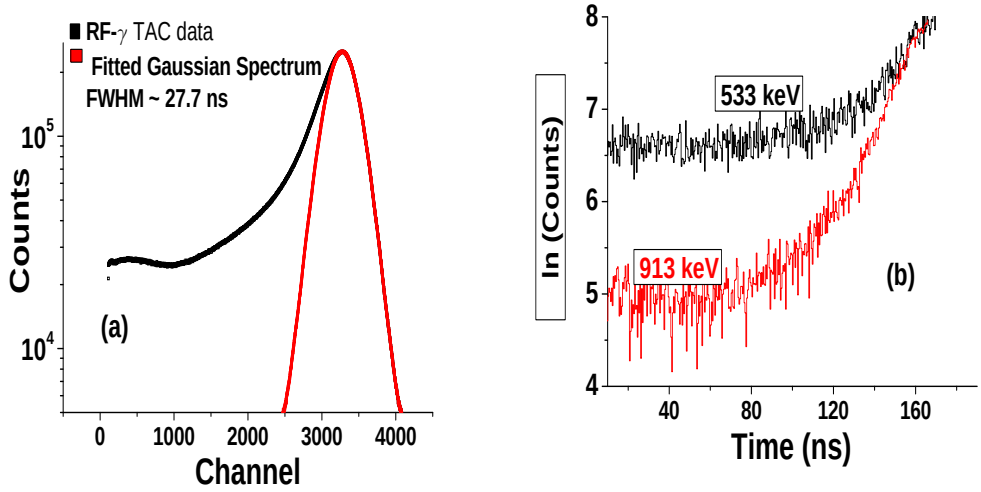

FIG. 4: (Color Online) (a) The RF-γ TAC spectrum without any gate on γ energies(left). (b) (Right) Comparison of RF-γ TAC spectra gated by 913 keV prompt transition and 533 keV delayed transition decaying from the isomer at 2772 keV through 36 keV. The logarithmic (ln) values of counts (to the base e) are plotted against time (ns) for ease of comparison.

mer at 2772 keV have also been observed and confirmed in this work (Fig. 6). However, in most of the cases their intensities could not be determined unambiguously. Thus the figure (Fig. 6) does not contain the intensities of these transitions.

Symmetric γ - γ matrix has been used to place different gamma transitions in the level scheme. To assign the spins and parities of the levels, the conventional DCO and polarization measurements have been performed. The relative intensities of these transitions have been obtained from 913-keV gated spectrum and relative intensities are normalized with respect to the intensity of 363 keV transition. The relative intensities, experimental R_{DCO} values, mixing ratios (for mixed transitions) and experimental polarization asymmetry values are listed in Table I. For transitions parallel to 913 keV transition, alternate gating transition has been considered to get intensities.

The intensities of transitions below the long-lived isomer at 2772 keV, are also determined from 200 ns time gated matrix. However, the ratios provided in Table II indicate that their intensities should increase by $\simeq$ 30% if they were measured from a matrix generated with 800 ns time gate. As expected, the angular correlation data for transitions below the isomer have been found to be isotropic with gates on transitions above the isomer. The intensities of gamma rays below the isomer in asymmetric matrix were quite low. Moreover, the excitation pattern is fragmented and contains many gamma rays of similar energies as those above the isomer. So it was also not possible to do correlation measurements of these transitions with gates on transitions below the isomer.

The relative intensities of most of the gamma rays in ^{153}Ho up to that of 466 keV gamma ray emitted from 7403 keV level, determined from the spectra gated by 913 keV gamma ray emitted from 2772 keV level, show good agreement with placements shown in Ref. [19]. However, the positions of 335 and 1001 keV gammas have been interchanged in the level scheme (Fig. 5) based on their intensities (Table I). The suggestion for reversal of the ordering of the 761- and 1042-keV transitions in Ref. [20] is not supported by the intensities of these transitions obtained in the present work. For low energy gammas like, 195 - , 140- keV transitions inclusion of internal conversion (IC) corrections have been important for proper placement. We have utilized IC coefficients obtained from online ICC calculator of BRICC [30].

Several isomers have been reported in ^{153}Ho in the earlier works [10, 19]. The relative intensities in the present work also provide information regarding the existing isomers. As two gamma transitions of 631 and 633 keV exist in the level scheme above and below the 2772 keV isomeric level, the intensities in Table I have been quoted with respect to that of 363 keV transition. Therefore any fall in intensity of gammas decaying from levels above the previously reported $\simeq$ 500ps isomer at 4679 keV level could not be observed. Moreover, this half life is also not comparable to 200ns prompt window selected for the time-gated symmetric matrix to be manifested in the decrease of intensity. For the reported 3 ns isomer [19] at 7598 keV, the relative intensity of 195 keV gamma transition decaying from it is $\simeq$ 75% compared to $\simeq$ 52% intensity of the 1001 keV gamma transition feeding this level, supporting the possibility of an isomer. Similarly, it is found that (Table I) the feeding to the 9074 keV state is highly fragmented. The several weak gamma transitions (796 keV, 1126 keV, 1185 keV and 1528 keV) feed this level. The level sequence above this state is also highly irregular. In the earlier work a $\simeq$ 300ps isomer was reported at this level. This sudden change in excitation pattern can also indicate presence of a structure isomer

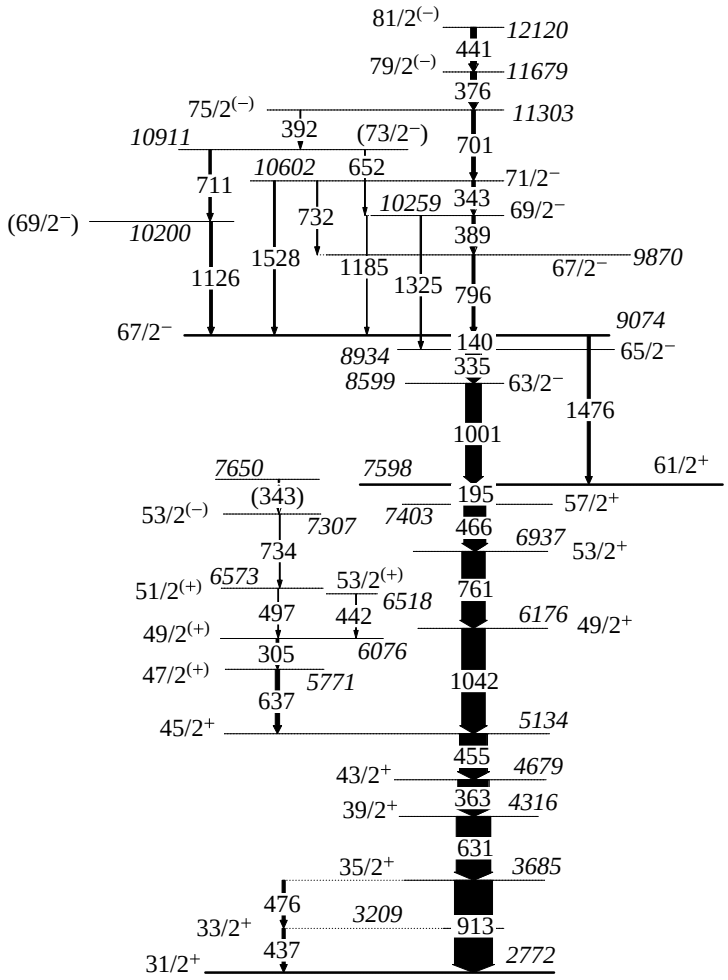

FIG. 5: Partial level scheme of ^{153}Ho

.

at this level.

For most of the gamma rays, the DCO and polarization results satisfy earlier assignments [1, 19]. However, for a few, some differences have been noted. In Ref. [19], 455 keV transition has been indicated as a M1 transition. The DCO measurement in the present work (Fig. 1) results to a value of $R_{DCO} = 1.07(3)$ from 90^o vs 40^o asymmetric matrix when gated by an E2 transition. The theoretical R_{DCO} values have been calculated by varying the mixing ratio to reproduce the experimental DCO ratio. This comparison indicated a large mixing ratio (E2/M1) (δ) 0.33(3) for this transition (Table I).

According to the present data analysis (Table I), 637 keV gamma transition is M1 in nature and the mixing ratio (δ) is 0.08, whereas it was previously mentioned [1, 19] as an E1 transition. The spin and parity assignments were not mentioned [1, 19] for 701, 376, 441 keV transitions. In the present work, it has been found that 701 and 376 keV transitions are of E2 character while 441 keV transition is M1 in nature. Previously, nature of 734 and 711 keV transitions were not specified [19]. Present measurement indicates that 734 keV and 711 keV transitions have E1 and E2 character, respectively (Table I).

B. Lifetime measurement

In Fig.7, RF-γ TACs correspond to, (i) 913 keV, a prompt gamma which decays from a state above the isomer at 2772 keV and (ii) the 533 keV gamma, which is emitted from a state just below the isomer. The decay curves clearly distinguish the two (Fig.7).

The lifetimes of the isomers have been determined by comparing a sequence of gamma gated TAC spectra and fitting them with one, two or three component exponential decay curves. The prompt RF- TAC spectrum generated with gate on 913 keV transition corresponds to a resolution of 15.23 $\pm$ 0.23 ns. For 533 keV, decaying from the isomer through 36 keV, the half-life comes out to be 251^{+54}_{-38} ns (Fig. 7).

A few other isomers, apart from this long lived isomer, have been reported in the earlier work [10, 19]. It has

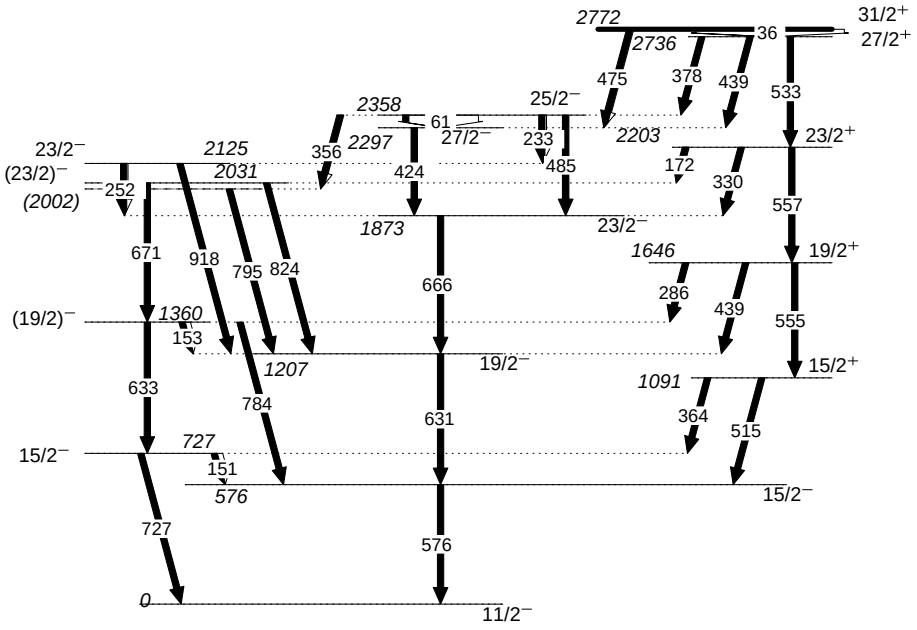

FIG. 6: Partial level scheme of ^{153}Ho below the isomer $31/2^+$ at 2772 keV

.

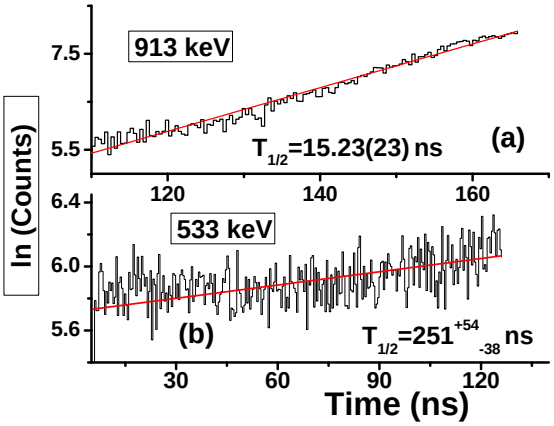

FIG. 7: (Color Online) Determination of (a)(top) prompt resolution of the TAC spectrum by fitting the decay curve of prompt 913 keV transition decaying from 3685 keV level, and (b) (bottom) the lifetime of the isomeric level at 2772 keV from the RF-γ TAC spectra gated by 533 keV transition. The logarithmic (ln) values of counts (to the base e) are plotted against time (ns) for ease of fitting.

been discussed already that the relative intensities of the transitions in the coincidence spectra gated by a transition below the isomers have been utilized to reconfirm their presence qualitatively.

For confirming these isomers further [10, 19] and to search for new isomers, another technique has been adopted. It has been mentioned earlier that two time-gated symmetric matrices with 200 ns and 800 ns gates in the $\gamma-\gamma$ time spectra have been generated. In the Table II, ratios of intensities of different γs (I_γ) in 913 keV gated spectra from 200ns and 800ns time matrices are tabulated. It is demonstrated that for the γ's below the long-lived isomer ($T_{1/2} > 200ns$), this ratio is $\approx$ 0.66-0.78 indicating their increased yield in the spectra generated from 800ns matrix. On the other hand for prompt gammas, this ratio ranges from 0.94-0.98. However, at several parts of the level scheme, gamma rays of similar energies exist above and below the $\simeq$ 200 ns isomer. For example, the intensity ratios of 363 and 631 keV gammas can not used for validating isomers as at least two gamma rays of similar energies are emitted from levels above and below the long-lived isomer. Systematic comparison of these ratios also indicates existence of a relatively longer lived isomer (>300 ps as reported in [19] at 9074 keV). For

TABLE I: Relative Intensity (I_{rel}), R_{DCO}, Δ_{IPDCO} and the mixing ratio (δ) of the γ transitions in ^{153}Ho.

E_γ(keV)	J_i^π	J_f^π	I_{rel}	E_{gate}(keV)	R_{DCO}	δ	Δ_{IPDCO}
140	$67/2^-$	$65/2^-$	32.72	913[E2]	1.21(9)	$0.20^{+0.09}_{-0.05}$	
195	$61/2^+$	$57/2^+$	75.38	913[E2]	0.96(3)	E2	0.11(1)
233[a]	$25/2^-$	$23/2^-$	6.80				
252[a]	$23/2^-$	$23/2^-$	4.66				
287[a]	$19/2^+$	$(19/2)^-$	4.82				
305	$49/2^{(+)}$	$47/2^{(+)}$	7.97	913[E2]	1.38(8)	$0.11^{+0.11}_{-0.05}$	-0.15(1)
335	$65/2^-$	$63/2^-$	48.45	913[E2]	1.39(6)	0.10(3)	-0.03(3)
343	$71/2^-$	$69/2^-$	11.05	761[E2]	1.24(3)	$0.19^{+0.09}_{-0.08}$	-0.07(3)
363	$43/2^+$	$39/2^+$	100	913[E2]	0.86(2)	E2	0.18(3)
376	$79/2^{(-)}$	$75/2^{(-)}$	19.12	913[E2]	0.89(8)	E2	0.04(8)
378[a]	$27/2^+$	$25/2^-$	22.17				
389	$69/2^-$	$67/2^-$	9.68	466[E2]	1.27(4)	$0.17^{+0.11}_{-0.08}$	-0.02(3)
424[a]	$27/2^-$	$23/2^-$	5.91				
441[b]	$81/2^{(-)}$	$79/2^{(-)}$	18.04	913[E2]	1.59(3)		-0.01(.10)
455	$45/2^+$	$43/2^+$	88.68	913[E2]	1.07(3)	0.33(3)	0.09(2)
466	$57/2^+$	$53/2^+$	71.06	913[E2]	0.84(3)	E2	0.08(2)
497	$51/2^{(+)}$	$49/2^{(+)}$	2.44	637[M1]	0.79(4)	0.3(5)	-0.01(5)
515[a]	$15/2^+$	$15/2^-$	13.87				
533[a]	$27/2^+$	$23/2^+$	33.12				
557[a]	$23/2^+$	$19/2^+$	52.35				
576[a]	$15/2^-$	$11/2^-$	36.15				
631	$39/2^+$	$35/2^+$	113.08	913[E2]	0.91(3)	E2	0.02(2)
637	$47/2^{(+)}$	$45/2^+$	14.13	913[E2]	1.43(1)	$0.08^{+0.12}_{-0.09}$	-0.17(8)
666[a]	$23/2^-$	$19/2^-$	8.31				
701	$75/2^{(-)}$	$71/2^-$	12.03	913[E2]	1.03(1)	E2	0.10(8)
711	$73/2^-$	$69/2^-$	7.87	1001[E1]	0.62(7)	E2	0.03(8)
727[a]	$15/2^-$	$11/2^-$	11.99				
732	$71/2^-$	$67/2^-$	3.65	1001[E1]	0.31(2)	E2	
734	$53/2^{(-)}$	$51/2^{(+)}$	2.93	637[M1]	0.85(3)	E1	0.42(4)
761	$53/2^+$	$49/2^+$	76.77	913[E2]	0.89(3)	E2	0.01(2)
783[a]	$(19/2)^-$	$15/2^-$	3.86				
796	$67/2^-$	$67/2^-$	9.68	913[E2]	1.11(8)		-0.03(2)
918[a]	$23/2^-$	$19/2^-$	8.26				
1001	$63/2^-$	$61/2^+$	51.79	913[E2]	1.24(7)	$0.19^{+0.05}_{-0.04}$	0.05(2)
1042	$49/2^+$	$45/2^+$	77.27	913[E2]	0.99(3)	E2	0.02(3)
1126	$69/2^-$	$67/2^-$	9.02	1001[E1]	1.02(4)	0.17	-0.11(1)
1185	$69/2^-$	$67/2^-$	1.89				
1325	$69/2^-$	$65/2^-$	4.60	1001[E1]	0.56(9)	E2	0.02(8)
1476	$67/2^-$	$61/2^+$	5.74				
1528	$71/2^-$	$67/2^-$	6.09	1001[E1]	0.42(7)	E2	

[a]Below the isomer

[b]May contain contribution from 442 keV ($53/2^{(+)} \rightarrow 49/2^{(+)}$)

transitions emitted from levels above 9074 keV in coincidence with 140 keV gamma decaying from 9074 keV state, the ratios lie between 0.81-0.93 (Table II). A comparison of these ratios with those corresponding to the isomer at 2772 keV indicates that the lifetime of the isomer at 9074 keV will be around 50 ns, instead of $\simeq 300ps$ as reported in [19].

TABLE II: Ratio of intensity (I_γ) in 913 keV gated spectra from 200ns and 800ns time matrices for γ - ray transitions in ^{153}Ho. Gammas below and above the long -lived isomer have been indicated as L and U, respectively. The 195 keV emitted from the 3 ns isomer at 7598 keV is indicated by I. The 140 keV gamma from the new isomer has been marked as N. $U140$ indicates gammas emitted from states above 9074 keV state in coincidence with 140keV gamma decaying from this state.

E_γ(keV)	Intensity(I_γ)		Ratio of I_γs (200ns/800ns)	Comment
	200ns	800ns		
378	8566	10352	0.83	L+U
701	6946	7564	0.92	U140
711	5074	5973	0.85	SU140
343	5163	5541	0.93	U140
389	4045	4609	0.88	U140
734	1986	2260	0.88	732 at U140
1528	1693	1941	0.87	U140
796	6005	6453	0.93	U140
1185	1392	1716	0.81	U140
1126	5578	6230	0.89	U140
1326	2614	2771	0.94	U140 but bypass 140
1476	1885	2240	0.84	U140
140	9164	10457	0.87	N
1001	31392	32872	0.95	U
335	24849	26834	0.93	U
195	36258	37697	0.96	I
497	1972	2210	0.89	U
305	5512	5629	0.98	U
442	8671	9848	0.88	U+U140
637	6597	7019	0.94	U
466	38900	41260	0.94	U
761	41609	43533	0.95	U
1042	46346	49211	0.94	U
455	48853	52600	0.93	U
363	56562	62031	0.91	U+L
631	56652	62900	0.90	L+U
475	1377	1964	0.70	L
533	10269	13303	0.77	L
557	15669	21518	0.73	L
515	3988	5409	0.74	L
576	11913	17014	0.70	L
439	9268	11931	0.78	L
424	2394	3152	0.76	L
233	3001	4509	0.66	L
252	1706	7043	0.72	L
918	2449	3402	0.72	L
666	3017	4246	0.71	L
727	4109	5426	0.76	L

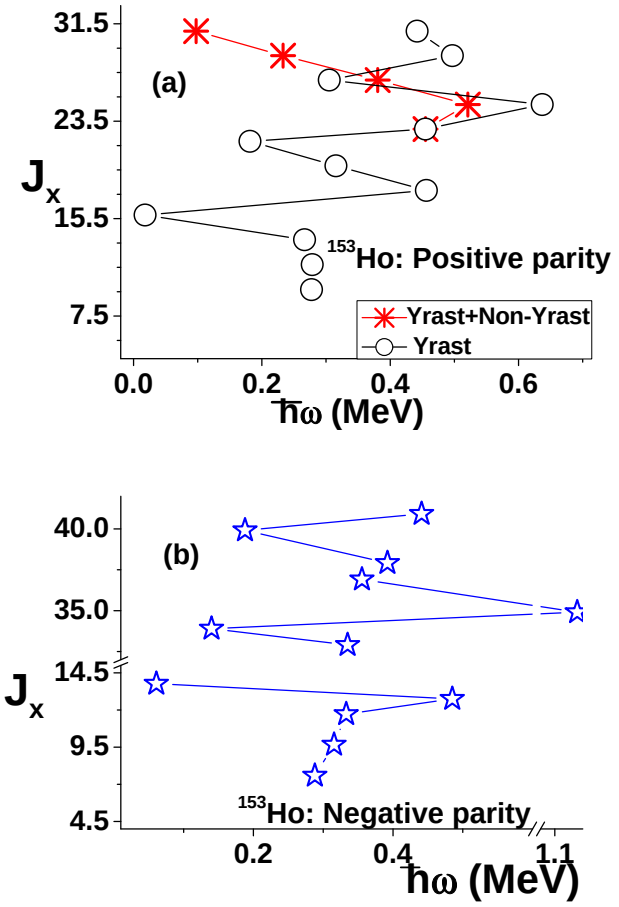

FIG. 8: (Color Online) The alignment plots for (a) positive and (b) negative parity states in ^{153}Ho

IV. DISCUSSIONS AND THEORETICAL CALCULATIONS

The structure of this nucleus poses a few interesting features as discussed below.

- Several isomers have been reported earlier [19] in the level scheme. They are similar to the yrast traps observed frequently in the nuclei in this mass region. The study of these isomers will be useful to follow the evolution of the structure of this nucleus with increasing excitation energy and spin.

- The negative parity states are distributed unevenly in the scheme. After $27/2^-$, the next negative parity states are observed at spin $53/2^{(-)}$ and then at spin $63/2^-$. These large gaps in spins for negative parity states are interesting and need special attention.

- For the positive parity $49/2^+$ and $53/2^+$ levels, the preferred deexcitation path includes the non-yrast

$49/2_2^+$ and $53/2_2^+$, which contradicts normal expectation. This needs special attention and theoretical interpretation.

- The level scheme apparently is not regular and it has been emphasized earlier [19] that the non-collective character of the motion manifests itself in this irregularity. However, in neighboring Dy isotopes, non-yrast collective states have been found to coexist with non-collective yrast states. So whether Ho also follows this trend or not needs to be understood phenomenologically as well as utilizing reliable theory.

The alignment plot of the positive and negative parity bands are shown in Fig. 8. Here J_x has been calculated using the expression $J_x = \sqrt{(J(J+1) - K^2)}$. Positive parity band has been plotted taking K=7/2, whereas for negative parity band, K=5/2 has been considered. These figures are useful to reveal the structural features.

- For the positive parity states, up to $45/2^+$ state the excitation pattern consists of several twists and turns indicating several changes in structure. Interestingly most of the bends are associated with isomers. The longest life isomer is at the first bend ($J_x \simeq 15.5$).

- At $45/2^+$, the excitation scheme bifurcates, the yrast branch is irregular indicating single particle alignment, whereas the non-yrast one is more regular and probably signify collective structure.

- The negative parity states show smooth increase in alignment till $23/2^-$. Beyond that the alignment is irregular, indicating single particle mode of angular momentum generation.

- A large discontinuity in alignment is observed beyond $27/2^-$ state. The next negative parity state has a spin $53/2(^-)$, about 13 units of angular momentum is gained.

The structure of this nucleus has been studied theoretically using two models. The issue of searching for energetically most stable shape at each angular momentum has been understood by calculating total Routhian surfaces [31] at different angular momenta. Moreover, a version of Particle Rotor Model [32, 33] has been utilized to calculate energies and transition probabilities of specific states.

A. TRS Calculations

The Total Routhian Surface (TRS) calculations [31] with a Woods - Saxon potential and monopole pairing predict a near-prolate deformation of $\beta_2 \simeq 0.20$ for this nucleus. As observed in Figs.9,10, at low frequencies with $\hbar\omega$ = 0.20 - 0.24 MeV, both the negative and positive parity states favor prolate deformation. However, at $\hbar\omega = 0.25$ MeV, shown for positive parity states (Fig. 9), there is a sudden transition to oblate shape as the most favored one. At higher rotational frequencies, the oblate shape remains energetically favored for both the parities (Figs. 9,10). This can be associated with the rotation alignment of a pair of $i_{13/2}$ neutrons, increasing the angular momentum from J $\simeq$ 9 to 21, over a small rotational frequency range of 0.25 to 0.28 MeV, contributing 12 units of angular momentum. These observations have been important while extending our studies using PRM.

The presence of several positive parity single particle states near the Fermi level smoothens shape transition and shape coexistence is observed (Fig. 9). However, for negative parity, single particle orbitals arising only from intruder $1h_{11/2}$ state are available. The shape transition therefore is drastic here and it also possibly leads to large gap in the available negative parity states in the spectrum in the band crossing region as predicted by TRS calculations (Fig. 10). There may be other negative parity states in the spin gap which has almost no overlap with higher spin negative parity states. Possibly they are not populated in the present heavy-ion fusion evaporation reaction for this reason.

B. PRM Calculations

To calculate specific energies and transition probabilities of different levels, PRM calculations have been done. The particular version of the model [32, 33] is discussed below.

1. Formalism

The model is based on the assumption that the nucleus under consideration is axially symmetric. In this model, the motion of an unpaired quasiparticle in a Nilsson deformed orbit is coupled to the rotational motion of the core through Coriolis interaction. We have used a version of the PRM [32, 33] in which the experimental core energies can be fed directly as input parameters.

The Hamiltonian of the odd-A system can be written as

$$H = H^0_{qp} + c\mathbf{R}.\mathbf{j} + E_c(R) \tag{3}$$

The first term is the Hamiltonian of a single quasiparticle. The quasiparticle (quasiproton, in the present case) is assumed to be moving in an axially symmetric Nilsson potential under the influence of BCS pairing. The pairing gap and the Fermi level are represented by Δ and λ respectively.

The total Hamiltonian is then diagonalize, giving the energy eigenvalues and the wave functions of the final

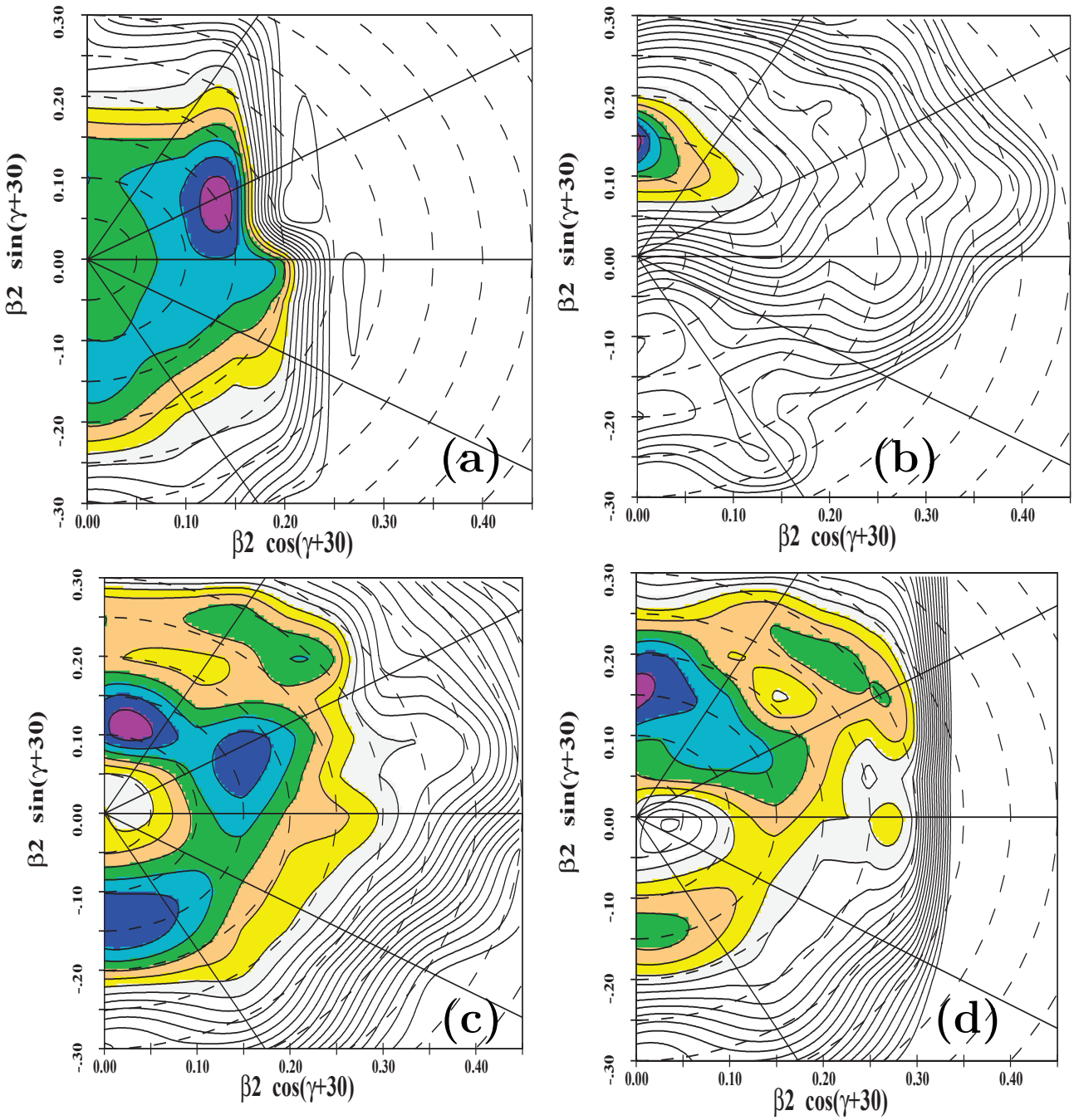

FIG. 9: (Color Online) TRS plots for the positive parity states. In the top row the plots correspond to (a)$\hbar\omega$ =0.2 (left) and (b) 0.40 (right) MeV (with $J \simeq 2.5$ and 37.5, respectively). In the bottom row, they are calculated for (c) $\hbar\omega = 0.25$ and (d) 0.28 MeV, (with $J \simeq 9.5$ and 21.5, respectively). Shape coexistence at ω=0.25 MeV is clearly indicated with yrast oblate and non-yrast prolate minimum.

states $|JM>$ in terms of the Coriolis mixing amplitudes f_{JK} and the basis states $|JMK>$:

$$|JM>=\sum_K f_{JK}|JMK> \qquad (4)$$

In the present version of the model [33], to identify the rotational composition of the final state $|JM>$, these states are expanded in terms of states with sharp R and j:

$$|JM>=\sum_{jR}\sum_K f_{JK}\alpha^{(K)}_{jR}|JMjR>, \qquad (5)$$

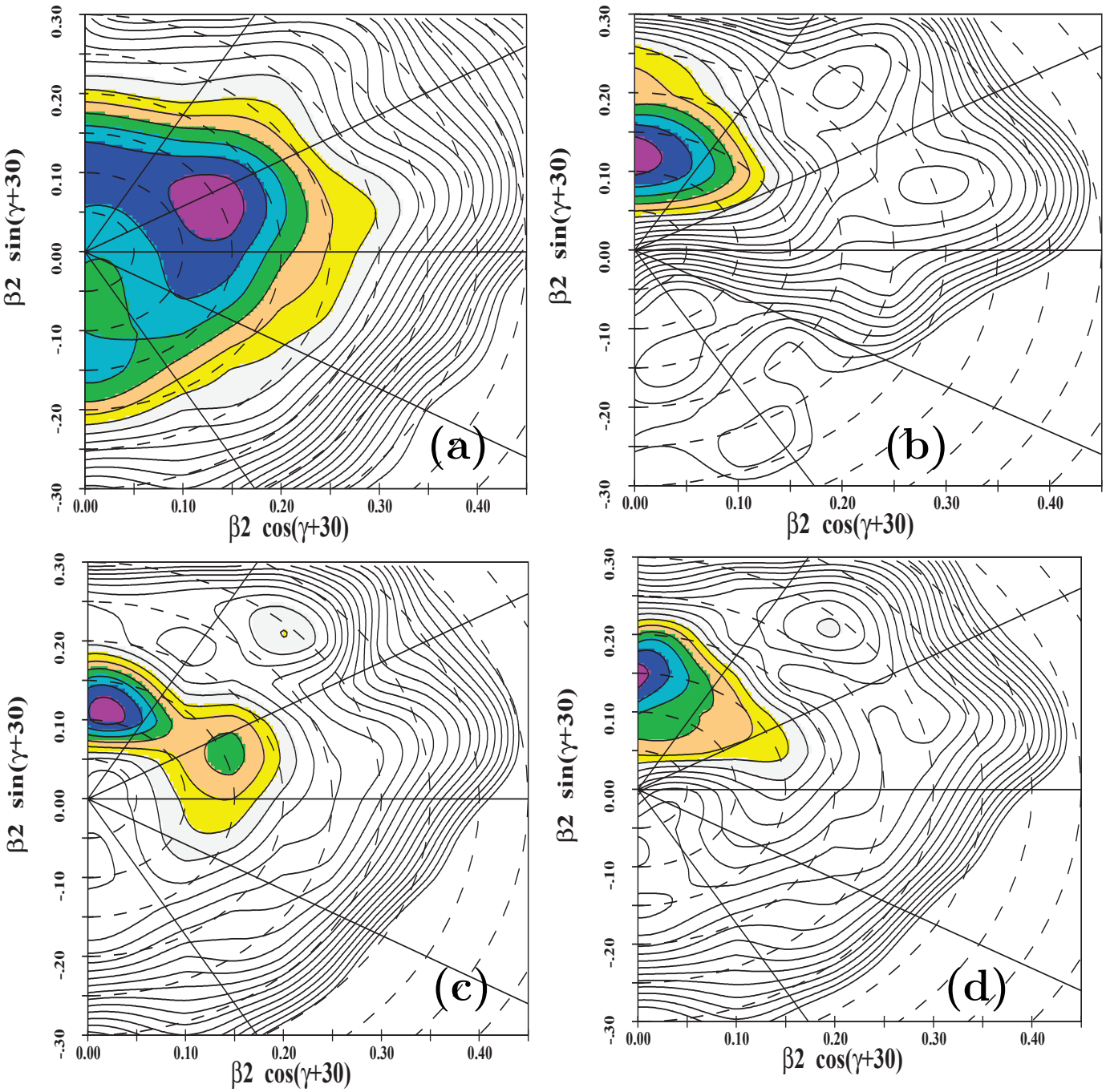

FIG. 10: (Color Online) TRS plots for the negative parity states. The plots correspond to (i) Top Row: (a) $\hbar\omega$ =0.2 (left) and (b) 0.45 MeV(right),(with $J \simeq 6.5$ and 32.5, respectively). (ii) Bottom row: (c) $\hbar\omega$ =0.25 (left) and (d) 0.28 (right) MeV,(with $J \simeq 12.5$ and 24.5, respectively)

where

$$\alpha_{jR}^{(K)} = \sqrt{2} \begin{bmatrix} J & j & R \\ K & -K & 0 \end{bmatrix} \tag{6}$$

So to calculate a state with total angular momentum J, where the single-particle angular momentum involved is j (say), the experimental core energies required will be given by the following range of R values:

$$R_{max} = J + j, \tag{7}$$

$$R_{min} = J - j. \tag{8}$$

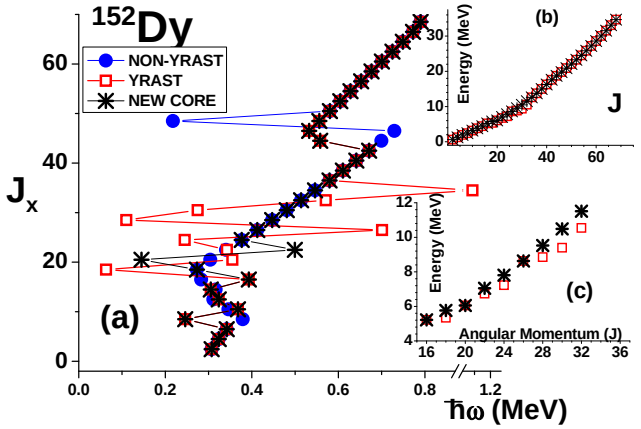

FIG. 11: (Color Online) (a) The alignment plot shows the yrast, nonyrast states of ^{152}Dy. The core states (*newcore*) selected for our calculations are indicated by stars. For all cases K=0 value has been considered for alignment calculation. (b) Experimental energy spectra of ^{152}Dy as a function of angular momentum (J). (c) The figure shows an expanded view of the region where vibration and rotational features compete and coexist.

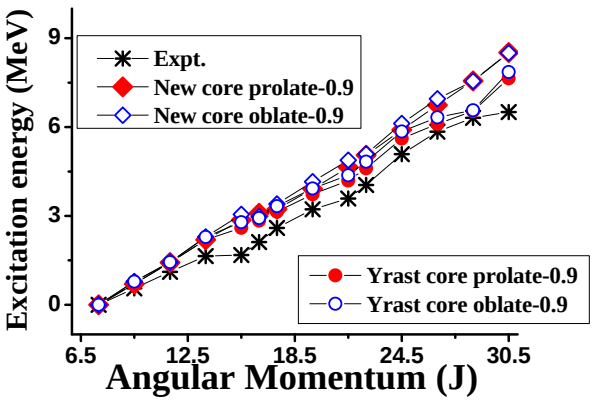

FIG. 12: (Color Online) The energy vs angular momentum plots for the positive parity states for different shape options with yrast and new cores.

2. Parameter choice

There are several parameters involved in the PRM calculations. The single-particle Nilsson parameters μ and κ (= 0.5920 and 0.065, respectively), have been deduced from the expression provided by Nilsson *et al.* [34]. The deformation parameter for the odd nucleus is chosen from the systematics of the experimentally deduced values in the neighboring even isotopes [35], which agrees quite well with the deformation (β_2) obtained from the TRS calculations (Figs. 9, 10). In our calculations, $\delta(= 0.95\beta_2) = \pm 0.14$. The pairing gap Δ is deduced from the experimental odd-even mass difference (Δ_{o-e}) calculated from mass data [36]. In our case, the experimental odd-even mass difference $\Delta_{o-e} = 1.5$ MeV. For positive (negative) parity states, all Nilsson single quasiparticle states from N=4 (N=5) have been considered. We have selected the Fermi level λ in such a way that it remains consistent with the observed ground state spin. We have calculated the energy spectra with the Fermi level at $\lambda = 43.8$ MeV, for both positive and negative parity states. For positive parity, it lies close to $3/2^+[411]$ and $3/2^+[422]$ orbitals originating primarily from $2d_{5/2}$ and $1g_{7/2}$ spherical states, respectively. The Fermi level is near $5/2^-[532]$ Nilsson orbital originating from $1h_{11/2}$ for negative parity states.

Here, the only adjustable parameter is Coriolis attenuation coefficient α. For ^{153}Ho nucleus, α is taken to be 0.90 and 0.99 for positive and negative parity bands, respectively. While calculating transition probabilities, for electric transitions effective charge $e_{eff} = 1.0$ have been used. Intrinsic quadrupole moment (Q_0) is necessary for these calculations has been provided from experimental quadrupole moment of ^{152}Dy [35]. For magnetic transitions, free values of g_l and g_s have been used.

3. *Choice of Core Energies*

The core energies are usually taken as the excitation energies of the yrast band of the neighboring even isotope. The ^{153}Ho nucleus is represented as an odd proton coupled to a ^{152}Dy core. In the present work, the level energies of the yrast spectra of ^{152}Dy are used as core energies.

While choosing the yrast spectra of Dy shown in Fig. 11, it is found that it has an interesting feature, the core possesses rotational as well as vibrational character [4]. Although at certain angular momentum the vibrational core states are yrast, the states populated via heavy ion fusion evaporation reaction also deexcites via nonyrast states which are members of the rotational band [1]. Two parallel branches of excitation scheme are observed, mildly collective and non-collective states are prevalent at low spins, at higher spins the coexisting non yrast states show collective behavior [4]. This is similar to the parallel branches observed in ^{153}Ho (Fg. 5) for spins $49/2^+$ and $53/2^+$ (Fig. 8).

The TRS calculations have been useful in this regard suggesting shape coexistence at certain angular frequency in ^{153}Ho. These results suggested that the alignment of $i_{13/2}$ neutrons are responsible for shape changes in ^{153}Ho. So the shape coexistence observed in even- proton nucleus ^{152}Dy [4] caused by neutron alignment is also manifested in neighboring odd-proton ^{153}Ho. Usually, the PRM calculations are not supposed to reproduce alignment effects. However, it has been demonstrated earlier [33] that, if the backbending (bb) is observed in the core for neutron (proton) alignment, for neighboring odd- pro-

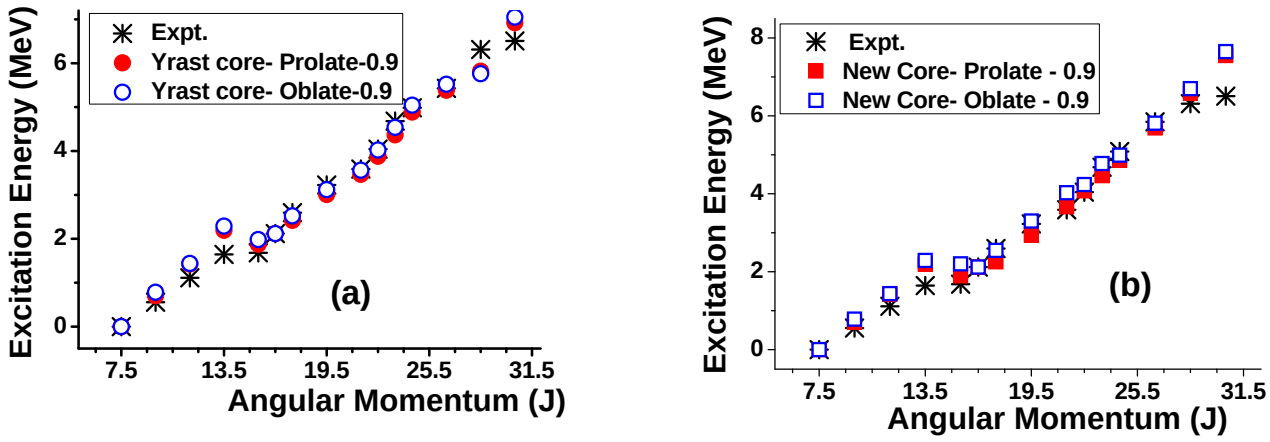

FIG. 13: (Color Online) The energy vs angular momentum plots for the positive parity states for different shape options. a) Results from calculations with yrast core compared with experimental yrast states. (b) Results from calculations with *newcore* compared with experimental states including nonyrast $49/2_2^+$ and $53/2_2^+$.

ton (neutron) nucleus, the backbending is reproduced using the present version of PRM provided the input core states included the backbending. This shape transition can be reproduced theoretically by this version of PRM, provided the proper core states are included in the calculation.

Therefore, spectra for ^{153}Ho have been calculated considering only yrast states of the core (indicated as *yrast*) and both the yrast states and non yrast rotational states of the core, indicated as *newcore*(Fig. 11). Calculations were performed with prolate as well as oblate deformation for the single particle Nilsson potential (Figs. 12, 13). In Table III, Table IV and Table V, the results for B(E2)s, branching ratios and mixing coefficients, respectively of several gamma transitions have been compared with experimental values.

C. Positive-parity states

We have shown the results for the positive parity states in Fig. 12. It is noted that above $23/2^+$, all states are somewhat over predicted with both the cores. For lower spin states, results for both prolate and oblate structure are almost same for both the cores.

However, we found that only if the states above the isomeric state $31/2^+$ are isolated from the set below, and the results are normalized to the energy of $33/2^+$ state, the normalized results match reasonably well with the experimental data (Fig. 13). This indicates structural differences between states above and below the isomer. Specific deformations which give best agreement at different spins have been discussed below in detail.

1. *Excitation energies as a function of spin (with normalization at $33/2^+$) and transition probabilities*

- For yrast core, the strongly populated $49/2_2^+$ and $53/2_2^+$ states (the decay out gamma transition energies are 761 and 1042 keV, respectively) are non yrast positive parity states (Fig. 5). It has been found that the high spin yrast positive parity states upto $49/2_1^+$ state have better agreement with oblate structure (Fig. 13a). Although the prolate option also reproduces the results well. Theoretical energies for $53/2_2^+$, $59/2_1^+$ and $61/2_1^+$ states deviate from experimental values. However, the B(E2) value extracted from the lifetime of $61/2_1^+$ state decaying by 195 keV gamma is reproduced well by the prolate option of this calculation (Table III).

- In new - core calculation (Fig. 13b), in which some of the non-yrast core states are taken as input, theoretical energies for $49/2_1^+$ and $53/2_1^+$ states have been compared with the experimental $49/2_2^+$ and $53/2_2^+$ states. The agreement is reasonably better till $39/2^+$ with oblate deformation. For $43/2^+$, $45/2^+$ and $47/2^+$ states, prolate deformation is favored. Both prolate and oblate deformation give almost similar agreement for $49/2_2^+$ and $53/2_2^+$. The calculated energy for $59/2_1^+$ with prolate deformation agrees quite well to experiment . The lifetimes of the $31/2^+$ and $43/2^+$ states decaying by 36 keV and 363 keV gammas, respectively, are reproduced best by the prolate and oblate deformation (Table III). So the theoretical results also (Table III) indicate that the $31/2^+$ state is a long-lived isomer. For $61/2_1^+$ state decaying by 195 keV gamma, results (energies as well as lifetimes) for both deformation worsens further compared to yrast core (Fig. 13a).

TABLE III: Comparison of experimental and theoretical reduced transition probabilities (B(E2)s in (e^2b^2)). For experimental quantities, corresponding errors are included within parentheses. The average core angular momentum (R) corresponding to each state has also been tabulated for different options.

				Expt.[1, 19]		Theory							
						Yrast core				New core			
E_x	J_i	J_f	E_γ	$T_{1/2}$	B(E2)[a]	Prolate		Oblate		Prolate		Oblate	
(keV)			(keV)	(ns)	(e^2b^2)	B(E2)	$R_i(R_f)$	B(E2)	$R_i(R_f)$	B(E2)	$R_i(R_f)$	B(E2)	$R_i(R_f)$
2772	$31/2_1^+$	$27/2_1^+$	36	[b]251^{+54}_{-38}	0.015 (3)	0.0003	16.1(12.7)	0.0002	17.0(11.6)	0.014	15.9(12.6)	0.102	14.0(11.6)
4679	$43/2_1^+$	$39/2_1^+$	363	0.5 (2)	0.02 (1)	0.106	21.9(20.1)	0.007	22.9(20.4)	0.003	21.9(20.6)	0.029	22.6(21.1)
7598	$61/2_1^+$	$57/2_1^+$	195	2.95 (15)	0.052(3)	0.038	31.4(28.7)	0.001	30.7(30.5)	0.109	30.9(28.9)	0.117	32.5(30.5)
9074	$67/2_1^-$	$65/2_1^-$	140[c]	0.3 (1)	0.07(2)	0.001	33(32)	0.002	33(32)	0.001	33(32)	0.0006	33(32)

[a]extracted from experimental half-lives.
[b]From present work
[c]M1+E2 transition, mixing ratio =0.2

TABLE IV: Comparison of experimental and theoretical branching ratios from calculations with *newcore* for $57/2_1^+$ state to investigate the reason behind strong decay path through non-yrast states. Note that in this set, as some of the core states are non-yrast, experimental non-yrast 53/2 state is equivalent to theoretical yrast state. See text for details.

E_x	J_i	J_f	E_γ	Exp	New core	
					Prolate	Oblate
7403	$57/2_1^+$	$53/2_1^{+(theo)}(53/2_2^{+(expt)})$	466	100	$\simeq$100	$\simeq$ 100
7403	$57/2_1^+$	$53/2_2^{+(theo)}(53/2_1^{+(expt)})$	885	Not observed	2.07×10^{-5}	7.13×10^{-5}

- The contribution of the different core states in the composition of the states of interest in ^{153}Ho are tabulated in (Table III). The average core angular momentum value gives an idea about the most relevant core states for a particular state in the odd-A nucleus. As expected, unlike that for negative parity states (which only originate from intruder orbital $1h_{11/2}$ of N=5), for positive parity, this value changes for different options of deformation. This is due to the fact that the most important lowest energy positive parity single quasiparticle Nilsson states originate from all states of N=4, except, $1g_{9/2}$.

- While calculating the branching of the decay of 7403 keV $(57/2_1^{+(expt)})$ level in the calculation with new core, the branching to the 6937 keV $(53/2_2^{+(expt)})$ is 100% with extremely small branch populating 6518 keV $(53/2_1^{+(expt)})$ state (Table IV). This justifies the decay of the yrast state at 7403 keV to the non-yrast state 6937 keV $(53/2_2^{+(expt)})$.

- For the branch parallel to the main excitation scheme, consisting of $49/2_1^{(+)}$, $47/2_1^{(+)}$, $51/2_1^{(+)}$, $53/2_1^{(+)}$ etc the yrast states in the calculations with yrast core, reproduce the mixing ratios reasonably well (Table V). Interestingly, the large mixing of 455 keV gamma decaying from $45/2^+$ state has been reproduced by the prolate deformation option of the yrast core calculations.

TABLE V: Comparison of experimental and theoretical mixing ratios for different transitions in ^{153}Ho for yrast core.

E_x	J_i	J_f	E_γ	Exp	Yrast core	
					Prolate	Oblate
5134	$45/2_1^+$	$43/2_1^+$	455	0.33(3)	0.29	0.12
5771	$47/2_1^{(+)}$	$45/2_1^+$	637	$0.08^{+0.12}_{-0.09}$	1.62	0.02
6076	$49/2_1^{(+)}$	$47/2_1^{(+)}$	305	$0.11^{+0.11}_{-0.05}$	0.08	0.01
6573	$51/2_1^{(+)}$	$49/2_1^{(+)}$	497	0.3(5)	0.07	0.12

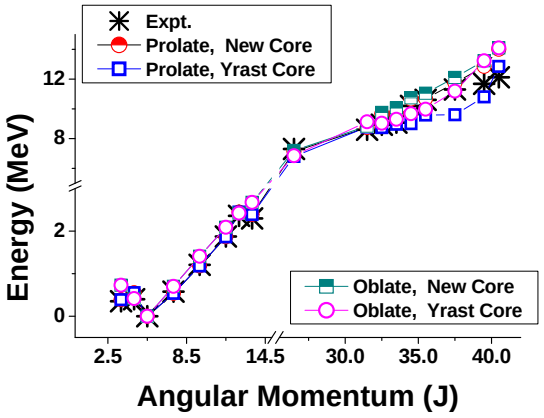

FIG. 14: (Color Online) Comparison of experimental and theoretical energies of negative parity states in ^{153}Ho

D. Excitation energies and transition probabilities of Negative-parity states

For negative parity levels, it is found that for lower spins the nucleus is prolate, which changes to an oblate structure at higher spins (Fig. 14) as expected from TRS calculations. For the PRM calculations, the choices of yrast or non-yrast cores do not make much difference in the results for these states. Only at the highest spins (81/2), prolate option appears to reproduce the energy better. For negative parity states, single quasiparticle Nilsson states near Fermi level originate only from intruder $1h_{11/2}$ (N=5), leading to relatively less fluctuations in core angular momentum for different options (Table III). Thereby making the results less sensitive to the change in the choice of core.

In the earlier work [19], a $\simeq$ 300 ps isomer has been reported at 9074 keV state decaying by 140 keV gamma, corresponding to a B(E2) value of 0.07 (2)e^2b^2 ($\simeq$ 659 e^2fm^4) (Table III) extracted utilizing the experimental mixing ratio determined in the present work (Table I). None of the calculations reproduce this B(E2) value. The predicted values are orders of magnitude smaller than the experimental value. These theoretical values correspond to longer half life for this state, ranging from around 10 ns (B(E2) =19.8 e^2fm^4) to 30 ns (B(E2) = 6.6 e^2fm^4). In the present work, definite experimental evidences have been discussed (Section IIIB) to indicate a longer half life ($\simeq$ 50 ns) for this state. The theoretical results also support this estimation from experimental observations.

V. SUMMARY AND CONCLUSION

The high-spin states in ^{153}Ho, have been populated by $^{139}_{57}La(^{20}Ne$, 6n) reaction at a projectile energy of 139 MeV at Variable Energy Cyclotron Centre (VECC), Kolkata, India. An earlier campaign of Indian National Gamma Array (INGA) setup has been utilized in this experiment. Data from gamma-gamma coincidence, directional correlation and polarization measurements have been analyzed to assign and confirm the spins and parities of the levels. We have also utilized the RF-gamma time spectrum to investigate the isomers in the excitation spectrum. A few additions and revisions of the reported level scheme of ^{153}Ho have been suggested. Lifetime of a high spin isomer has been suggested to be longer than the earlier result.

The alignment plots of the excitation spectra have been useful to understand the different modes of excitation phenomenologically. Theoretical calculations, both TRS and PRM have provided additional microscopic insight.

The regularity in the increase in alignment with angular frequency for low energies for both positive and negative parity states indicate mild collectivity. This is also supported by TRS results showing prolate minimum for low angular frequency. Although PRM calculations indicate similar agreement with energy values for both prolate and oblate options, the isomer lifetime at $31/2^+$ is best reproduced by a prolate deformation.

For positive parity this regularity is repeated till relatively higher spins with turns in between which may indicate intrinsic configuration changes. The PRM calculations reproduce $43/2^+$ lifetime by an oblate option and the $61/2^+$ lifetime by a prolate option.

The shape coexistence is clearly manifested in positive parity alignment plot with a smooth branch (non-yrast) and a irregular branch (yrast) beyond $45/2^+$. This is supported by PRM. The results for prolate deformation with *newcore* agree well with the non-yrast branch. This shape coexistence is also observed in TRS plots.

The higher spin negative parity states are erratic as shown in alignment plot. It also agrees well with PRM results for oblate deformation and supported by oblate minimum in TRS plot.

Future investigations are needed to improve the lifetime measurements to confirm the conclusions from this work on firmer ground.

Acknowledgment

The authors would like to acknowledge all INGA collaborators for their sincere help and cooperation. The authors sincerely thank P. K. Das (SINP) and the target laboratory of VECC, Kolkata, for preparation of the target. Special thanks are due to the Cyclotron staff of VECC for providing necessary beams during the experiment. This work is an outcome of the Collaborative Research Scheme (CRS) project of UGC-DAE Consortium for Scientific Research, Kolkata Centre. One of the authors (D.P.) acknowledges financial support from UGC-DAE-CSR-KC and IIEST, Shibpur, Howrah for providing research fellowship at different stages of this work.

[1] Data extracted using the NNDC On-line Data Service from the ENSDF database version of March 25, 2016.
[2] Kris Heyde, John L. Wood, Rev. of Mod. Phys, **83**, 1467 (2011).
[3] M.A. Bentley *et al.*, J. Phys. G: Nucl. Part. Phys. **17**, 481 (1991) and references therein.
[4] M. B. Smith *et al.*, Phys. Rev. C **61**, 034314 (2000) and references therein.
[5] J. Jastrzebski *et al.*, Phys. Lett. B **97**, 50 (1980).
[6] Ani Aprahamian and Yang Sun, Nature Physics **1**, 81 (2005) and references therein.
[7] C.T. Zhang *et al.*, Z. Phys. A **348**, 65 (1994).
[8] M. A. Rizzutto *et al.*, Phys. Rev. C **55**, 1130 (1997).
[9] S. Andre *et al.*, Nucl. Phys. A **575**, 155 (1994).
[10] R. G. Helmer, Nucl. Data Sheets **107**, 507 (2006).
[11] S.J. Chae *et al.*, Z. Phys. A **350**, 89 (1994).

[12] G. Dey *et al.*, Proc. DAE-BRNS Symp. Nucl. Phys. (India) **51**, 284 (2006), http://www.sympnp.org/proceedings/.
[13] A.Chakraborty *et al.*, Proc. DAE-BRNS Symp. Nucl. Phys. **53**, 249(2008), http://www.sympnp.org/proceedings/.
[14] Dibyadyuti Pramanik *et al.*, Proc. DAE-BRNS Symp. Nucl. Phys. **55**,14 (2010), http://www.sympnp.org/ proceedings/.
[15] Dibyadyuti Pramanik *et al.*, Proc. DAE-BRNS Symp. Nucl. Phys. **55**,74 (2010), http://www.sympnp.org/ proceedings/.
[16] Dibyadyuti Pramanik *et al.*, Proc. DAE-BRNS Symp. Nucl. Phys. **56**, 392 (2011), http://www.sympnp.org/ proceedings/.
[17] Dibyadyuti Pramanik *et al.*, Proc. DAE-BRNS Symp. Nucl. Phys. **57**, 212 (2012), http://www.sympnp.org/ proceedings/.
[18] Dibyadyuti Pramanik *et al.*, Proc. DAE-BRNS Symp. Nucl. Phys. **58**, 302 (2013), http://www.sympnp.org/ proceedings/.
[19] D.C. Radford *et al.*, Phys. Lett. B **126**, 24 (1983).
[20] D. E. Appelbe *et al.*, Phys. Rev. C **66**, 044305 (2002).
[21] G.D. Alkhazov *et al.*, Nucl. Phys.A **504**, 549 (1989).
[22] R. Raut *et al.*, Proc. DAE-BRNS Symp. Nucl. Phys. (India) **47B**, 578 (2004),http://www.sympnp.org/ proceedings/.
[23] Ranjan K. Bhowmik in *Structure of atomic nuclei*, proceedings of the SERC School, Puri, India, 1996, edited by L. Satpathy (Narosa Publishing House, New Delhi, 1999) p. 259.
[24] D. C. Radford, Nucl. Inst. Meths. A **361**, 297 (1995).
[25] E.S. Macias, W.D. Ruhter, D.C. Camp, R.G. Lanier, Comput. Phys. Commun. **11**, 75 (1976).
[26] Indrani Ray *et al.*, Phys. Rev. C **76**, 034315 (2007).
[27] Abhijit Bisoi *et al.*, Phys. Rev. C **89**, 024303 (2014).
[28] Abhijit Bisoi *et al.*, Phys. Rev. C **90**, 024328 (2014).
[29] S Rajbanshi *et al.*, Phys. Rev. C **89**, 014315 (2014).
[30] T. Kibedi, T.W. Burrows, M.B. Trzhaskovskaya, P.M. Davidson, C.W. Nestor, Jr., Nucl. Instr. and Meth. A **589**, 202 (2008), http://bricc.anu.edu.au/index.php.
[31] W. Nazarewicz, R. Wyss and A. Johnson, Nucl. Phys. A **503**, 285 (1989).
[32] E. M. Müller and U. Mosel, J. Phys. G **10**, 1523 (1984).
[33] M. Saha, A. Goswami, S. Bhattacharya, S. Sen, Phys. Rev. C **42**, 1386 (1990).
[34] S. G. Nilsson, C. F. Tsang, A. Sobiczewski, Z. Szymanski, S.Wycech, C. Gustafson, I. L. Lamm, P. Moller, and B. Nilsson, Nucl. Phys. A **131**, 1 (1969).
[35] S. Raman, C. W. Nestor, Jr., and P. Tikkanen, At. Data and Nucl. Data Tables **78**, 1 (2001).
[36] G. Audi *et al.,* Chinese Physics C **36**, 1157 (2012).